Journal of the Geological Society, London, Vol. **160**, 2003, pp. 385–399. Printed in Great Britain.

Exhumation history of eastern Ladakh revealed by $^{40}Ar/^{39}Ar$ and fission-track ages: the Indus River–Tso Morari transect, NW Himalaya

M. SCHLUP[1], A. CARTER[2], M. COSCA[1] & A. STECK[1]

[1]*Institut de Minéralogie et Géochimie, Université de Lausanne, 1015 Lausanne, Switzerland (e-mail: micha.schlup@img.unil.ch)*

[2]*London Thermochronological Research Group, Research School of Earth Sciences, Birkbeck and University College, Gower Street, London WC1E 6B, UK*

Abstract: Fission-track and $^{40}Ar/^{39}Ar$ ages place time constraints on the exhumation of the North Himalayan nappe stack, the Indus Suture Zone and Molasse, and the Transhimalayan Batholith in eastern Ladakh (NW India). Results from this and previous studies on a north–south transect passing near Tso Morari Lake suggest that the SW-directed North Himalayan nappe stack (comprising the Mata, Tetraogal and Tso Morari nappes) was emplaced and metamorphosed by *c*. 50–45 Ma, and exhumed to moderately shallow depths (*c*. 10 km) by *c*. 45–40 Ma. From the mid-Eocene to the present, exhumation continued at a steady and slow rate except for the root zone of the Tso Morari nappe, which cooled faster than the rest of the nappe stack. Rapid cooling occurred at *c*. 20 Ma and is linked to brittle deformation along the normal Ribil–Zildat Fault concomitant with extrusion of the Crystalline nappe in the south. Data from the Indus Molasse suggest that sediments were still being deposited during the Miocene.

Keywords: Himalaya, eastern Ladakh, $^{40}Ar/^{39}Ar$, fission-track dating, exhumation.

The aim of this study is to investigate the exhumation history of the Rupshu area in eastern Ladakh situated in NW India (Fig. 1; Berthelsen 1953; Gansser 1964; Thakur & Misra 1984; Hodges 2000), following detailed geological, structural and metamorphic studies carried out by researchers at the University of Lausanne since 1996 (Steck *et al*. 1998; Girard 2001). These workers recognized a new nappe stack formed by three SW-directed nappes: the Tso Morari, Tetraogal and Mata nappes. Meanwhile, detailed geological investigations conducted in the Indus Suture Zone and Molasse (Fuchs & Linner 1996) and new petrographic and thermobarometric data from the Tso Morari eclogites (discovered by Berthelsen 1953) were published (Fig. 2; De Sigoyer *et al*. 1997; Guillot *et al*. 1997). Geochronological data for the Tso Morari metamorphism, published by De Sigoyer *et al*. (2000), were used to constrain the time of continental subduction and collision; Lu–Hf and Sm–Nd methods were used to date metamorphism related to subduction and gave an age of *c*. 55 Ma, whereas timing of retrogression to amphibolite facies, related to collision, was estimated at *c*. 47 Ma by Sm–Nd, Rb–Sr and $^{40}Ar/^{39}Ar$ methods. In addition, $^{40}Ar/^{39}Ar$ cooling ages constrained the time of greenschist-facies retrogression in the Tso Morari dome to *c*. 30 Ma, which previously represented the only geochronological data available for the low-temperature thermal history of the North Himalayan nappe stack, which comprises the Mata, Nyimaling Tsarap, Tetraogal and Tso Morari nappes in NW India (Steck *et al*. 1993, 1998).

To further constrain the low-temperature history of eastern Ladakh we present fission-track (FT) and $^{40}Ar/^{39}Ar$ geochronological data from a north–south geological transect (Fig. 2). The apatite and zircon fission-track and $^{40}Ar/^{39}Ar$ ages permit us to reconstruct upper-crustal cooling through the temperature range of *c*. 500–60 °C. The transect begins close to Chumatang village on the Indus River, and ends in the Parang valley about 15 km south of Tso Morari Lake. The study area falls within the northern part of the transect investigated by Steck *et al*. (1998) and includes the Ladakh Batholith, Indus Molasse, Indus Suture Zone, and the Tso Morari, Tetraogal and Mata nappes.

Geological setting

The study area extends from the Trans-Himalayan Plutonic Belt (Honegger *et al*. 1982), through the Indus–Tsangpo Suture Zone (Gansser 1964) and the Indian Margin, to the internal parts of the Indian crust. The area contains several tectonic domains with contrasting tectonometamorphic histories (Fig. 2). From north to south, there is the Ladakh Batholith, Indus Molasse and Indus Suture Zone, and farther south, there is the North Himalayan nappe stack, which includes the Tso Morari, Tetraogal and Mata nappes in eastern Ladakh (Steck *et al*. 1998).

The Ladakh Batholith

The Ladakh Batholith is part of an Andean-type Trans-Himalayan plutonic belt extending from Afghanistan in the west, to east of Lhasa in Tibet (Honegger *et al*. 1982; Schärer *et al*. 1984; Sharma 1991; Weinberg & Dunlap 2000). Onset of plutonism, caused by partial melting of the mantle above the subducted Neo-Tethyan slab beneath the Eurasian margin, has been estimated to occur at 102 Ma in its NW section (Table 1; Honegger *et al*. 1982; Schärer *et al*. 1984). The magmatic activity ends at *c*. 50 Ma (Weinberg & Dunlap 2000), and marks the transition from subduction to continental collision. The occurrence of prehnite in mylonitized diorites at the top of the batholith reveals that the batholith was overthrust by the molasse under anchizonal metamorphic conditions. We infer from K/Ar illite ages between 40 and 35 Ma (Van Haver *et al*. 1986) that thrusting occurred during Late Eocene time.

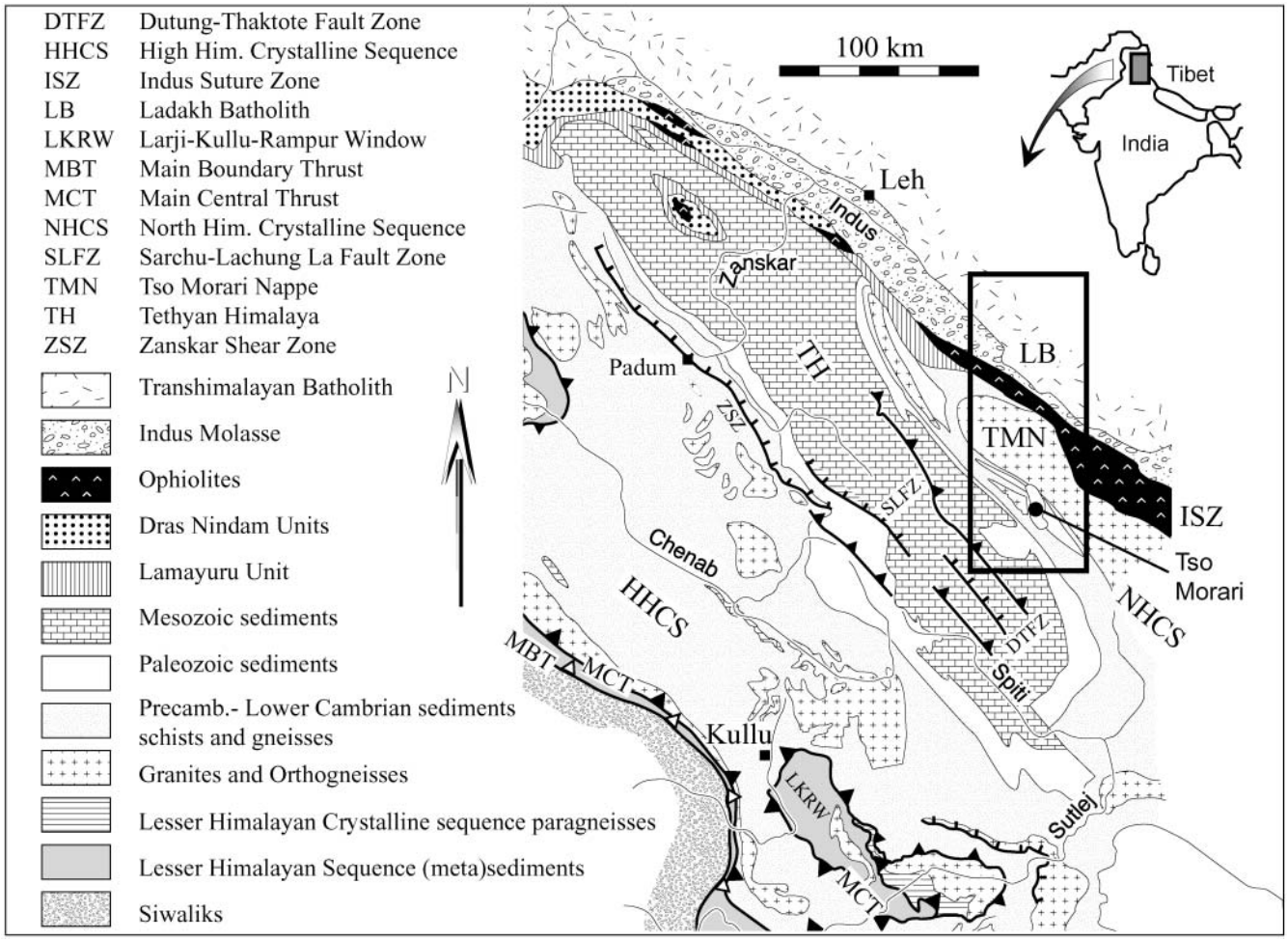

Fig. 1. Simplified geological map of NW India, between Kullu and Leh. Modified after Steck *et al*. (1993, 1998), Epard *et al*. (1995), Frank *et al*. (1995), Vannay & Grasemann (1998) and Girard (2001). The investigated area is indicated by the rectangle, and is shown enlarged in Figures 2 and 3.

The Indus and Chulze molasses

The Ladakh Batholith is overlain by Lower Tertiary sediments of the Indus Molasse (Garzanti & Van Haver 1988). In the study area, illite crystallinity values and well-preserved sedimentary structures suggest that the molasse has not undergone significant metamorphism. On its southern edge the Indus Molasse is overthrust by ophiolites of the Indus Suture Zone along the SW-dipping Nidar Thrust (Thakur & Virdi 1979).

In the internal part of the Indus Suture Zone, a detrital continental series, the Chulze Molasse, lie discordantly on the ophiolites (Fig. 2). De Sigoyer (1998) supposed that these series are of post-Eocene age. Illite crystallinity values reveal that metamorphism occurred under anchizonal conditions.

The Indus Suture Zone

The Indus Suture Zone (Fuchs & Linner 1996), also locally called the Sumdo Formation (Thakur & Virdi 1979), contains the well-preserved Nidar ophiolite and the Zildat Ophiolitic Mélange. Linner *et al*. (2001) estimated an age of 140.5 ± 5.3 Ma for the magmatic crystallization of ophiolites based on Sm–Nd data for plagioclase and clinopyroxene of one gabbro sample. The ophiolites are nearly undeformed and underwent low-grade metamorphism indicated by the occurrence of prehnite and pumpellyite in the gabbros.

The Zildat Ophiolitic Mélange underwent slightly higher-grade metamorphism as the Nidar ophiolite, under greenschist-facies conditions that occurred during the activation of a NE-dipping low-angle shear zone (Steck *et al*. 1998). This structure was later cut by the NE-dipping high-angle Ribil–Zildat normal fault (Virdi *et al*. 1977; Steck *et al*. 1998; Guillot *et al*. 2000) that juxtaposes the Zildat Ophiolitic Mélange with the roots of the Tso Morari nappe and the overlying higher structures of the Tetraogal and Mata nappes (Fig. 3).

Fig. 2. Simplified geological map compiled from Thakur & Misra (1984), Fuchs & Linner (1996), Steck *et al*. (1998) and Girard (2001), showing sample localities A–T. The $^{40}Ar/^{39}Ar$ and fission-track ages are given in Ma. Localities, techniques and errors are given in Tables 2–4 and in Figure 4. *P–T* paths for the various units were drawn following the mineral assemblages from the mafic rocks (after De Sigoyer *et al*. 1997; Steck *et al*. 1998; Mukherjee & Sachan 2001; Schlup 2003). Isograds for metapelites are related to the Barrovian-type metamorphism (drawn from Steck *et al*. (1998) and Girard (2001)). Am, amphibolite; BS, blueschist; Bt, biotite; Coe, coesite; EA, epidote–amphibolite; Ec, eclogite; Gr, granulite; GS, greenschist; Hb, hornblende; Pc-C, Precambrian–Cambrian; Ph, phengite; P-M, Permo-Mesozoic; PP, prehnite–pumpellyite; Qtz, quartz; Ze, zeolite.

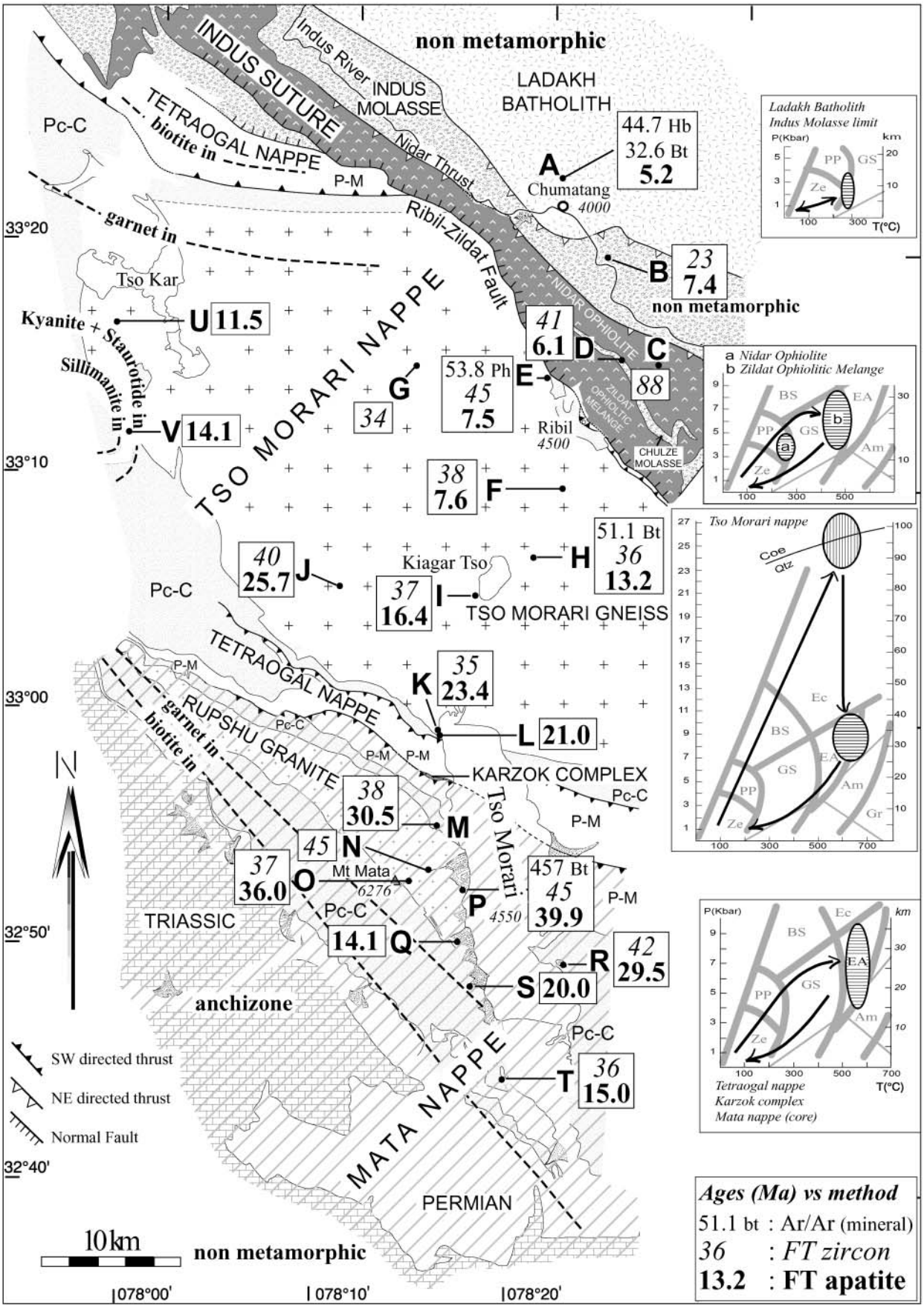
non metamorphic
INDUS SUTURE
Indus River
INDUS MOLASSE
LADAKH BATHOLITH
TETRAOGAL NAPPE
biotite in
Pc-C
P-M
Nidar Thrust
Ribil-Zildat Fault
44.7 Hb
32.6 Bt
5.2
A
Chumatang
4000
B
23
7.4
non metamorphic
33°20
garnet in
Tso Kar
Kyanite + Staurotide in
Sillimanite in
U 11.5
V 14.1
TSO MORARI NAPPE
G
34
53.8 Ph
45
7.5
E
41
6.1
D
C
88
NIDAR OPHIOLITE
ZILDAT OPHIOLITIC MELANGE
CHULZE MOLASSE
Ribil
4500
33°10
38
7.6
F
51.1 Bt
36
13.2
H
40
25.7
J
Kiagar Tso
37
16.4
I
TSO MORARI GNEISS
Pc-C
TETRAOGAL NAPPE
K
35
23.4
33°00
RUPSHU GRANITE
garnet in
biotite in
L 21.0
KARZOK COMPLEX
Pc-C
P-M
38
30.5
M
45
N
37
36.0
O
Mt Mata
6276
Tso Morari
457 Bt
45
39.9
P
4550
TRIASSIC
14.1
Q
R
42
29.5
S 20.0
anchizone
32°50'
Pc-C
T
36
15.0
MATA NAPPE
PERMIAN
SW directed thrust
NE directed thrust
Normal Fault
32°40'
10km
non metamorphic
078°00'
078°10'
078°20'
Ladakh Batholith
Indus Molasse limit
P(Kbar)
km
T(°C)
a Nidar Ophiolite
b Zildat Ophiolitic Melange
Tso Morari nappe
Coe
Qtz
Tetraogal nappe
Karzok complex
Mata nappe (core)
Ages (Ma) vs method
51.1 bt : Ar/Ar (mineral)
36 : FT zircon
13.2 : FT apatite

Table 1. *Synthesis of previous geochronological data related to the units studied in this work*

Unit	Location	Event	Age (Ma)	Method	References
Ladakh Batholith	Kargil	Granite crystallization	103 ± 3	U/Pb (zircon)	Honegger *et al*. (1982)
	Kargil	Granite crystallization	101 ± 2	U/Pb (zircon)	Schärer *et al*. (1984)
	Leh	Granite crystallization	49.8 ± 0.8	U/Pb (zircon)	Weinberg & Dunlap (2000)
	Leh	Cooling	48.7 ± 1.6	K/Ar (biotite)	Honegger *et al*. (1982)
	Leh	Cooling	45.7 ± 0.8	Ar/Ar (hornblende)	Weinberg & Dunlap (2000)
	Tangtse	Cooling	33.8 + 0.4	Ar/Ar (K-feldspar)*	Dunlap *et al*. (1998)
	Upshi	Cooling	28 ± 3	FT (apatite)	Sinclair & Jaffey (2001)
	Chumatang†	Cooling	7–9	FT (apatite)	Sharma & Choubey (1983)
Indus Molasse	Himis Shukpa	Metamorphism	35–40	K/Ar (phyllite)	Van Haver *et al*. (1986)
	Nimu	Cooling	14 ± 3	FT (apatite)	Sinclair & Jaffey (2001)
Indus Suture	Kalra Valley†	Gabbro crystallization	140.5 ± 5.3	Sm/Nd (Pl–Cpx)	Linner *et al*. (2001)
	Shergol	HP metamorphism	98.5 ± 0.5	K/Ar (glaucophane)	Honegger *et al*. (1989)
	North Pakistan	HP metamorphism	82.5 ± 2	Ar/Ar (phengite)	Maluski & Matte (1989)
Tso Morari nappe	Polokongka La†	Granite crystallization	479 ± 2	U/Pb (zircon)	Girard & Bussy (1999)
	Gyanbarma†	Granite crystallization	479 ± 2	U/Pb (zircon)	Girard & Bussy (1999)
	Kiagar La†	HP metamorphism	55 ± 7	Sm/Nd (Grt–Gln–WR)	De Sigoyer *et al*. (2000)
	Kiagar La†	HP metamorphism	55 ± 12	Lu/Hf (Grt–Cpx–WR)	De Sigoyer *et al*. (2000)
	Kiagar La†	HP metamorphism	55 ± 17	U/Pb (Aln)	De Sigoyer *et al*. (2000)
	Kiagar La†	Amphibolite metamorphism	48 ± 2	Ar/Ar (phengite)	De Sigoyer *et al*. (2000)
	Tso Morari†	Amphibolite metamorphism	47 ± 11	Sm/Nd (Grt–Amp–WR)	De Sigoyer *et al*. (2000)
	Tso Kar†	Amphibolite metamorphism	45 ± 4	Rb/Sr (Phe–Ap–WR)	De Sigoyer *et al*. (2000)
	Gyanbarma†	Cooling	31.1 ± 0.3	Ar/Ar (muscovite)	De Sigoyer *et al*. (2000)
	Gyanbarma†	Cooling	29.3 ± 0.3	Ar/Ar (biotite)	De Sigoyer *et al*. (2000)
	Gyanbarma†	Cooling	29 ± 0.4	Ar/Ar (biotite)	De Sigoyer *et al*. (2000)
Mata nappe	Kele†	Granite crystallization	482.5 ± 1	U/Pb (zircon)	Girard & Bussy (1999)
Tethyan Zone	Pin Valley, Spiti	Metamorphism	42–45	Ar/Ar (illite)	Wiesmayr & Grasemann (1999)

Aln, allanite; Amp, amphibole; Cpx, clinopyroxene; Gln, glaucophane; Grt, garnet; Phe, phengite; WR, whole rock.
*Ar/Ar K-feldspar is a minimum age in spectrum.
†Locations situated on the present transect.

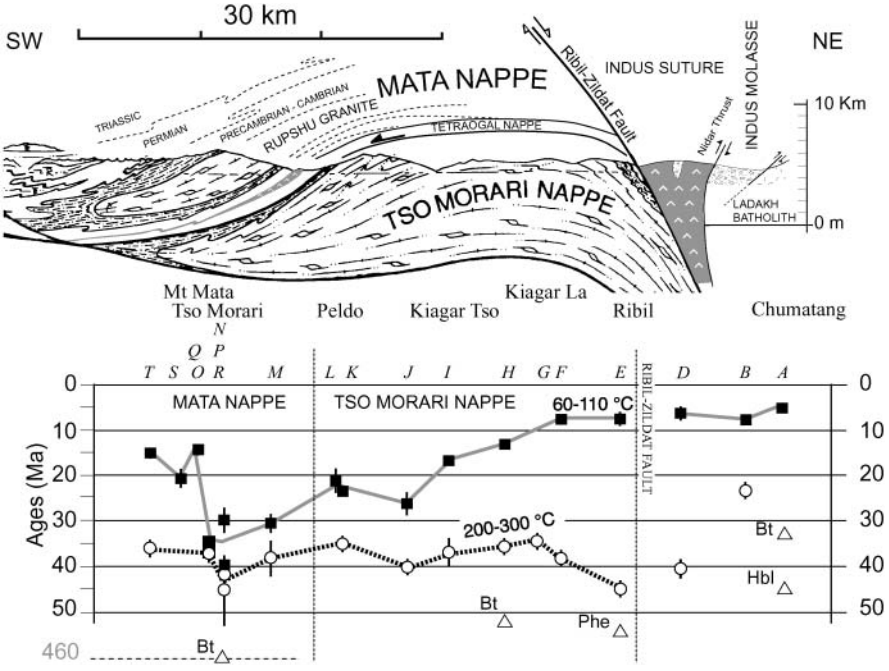

Fig. 3. Fission-track (FT) and $^{40}Ar/^{39}Ar$ ages projected along the Indus River–Tso Morari north–south transect. Modified after a geometric interpretation drawn from NE–SW cross-sections by Steck *et al*. (1998). △ with mineral abbreviations, $^{40}Ar/^{39}Ar$ ages (Bt, biotite; Hbl, hornblende; Phe, phengite); ○, zircon FT ages; ■, apatite FT ages. Given temperatures refer to the Partial Annealing Zones (PAZ) of zircon and apatite. Italic letters refer to sample identification used in Figure 2 and Tables 1 and 2. Error bars correspond to the standard error of the mean for FT ages (not plotted when the symbol is larger than the error bar).

The Tso Morari nappe

The Tso Morari nappe (Steck *et al*. 1998) consists of the Ordovician Tso Morari granite-gneiss (Table 1; Girard & Bussy 1999) and Precambrian to Cambrian sediments. The Tso Morari nappe originates from a slab of the North Indian margin that underthrust the North Indian crust below Asia to a depth of at least 90 km (De Sigoyer *et al*. 1997; Mukherjee & Sachan 2001) and is readily distinguished from the adjacent units by the presence of eclogites (Berthelsen 1953; Guillot *et al*. 1997). After HP–LT metamorphism estimated at *c*. 55 Ma (De Sigoyer *et al*. 2000), and probably because of buoyancy forces (Chemenda *et al*. 1995, 2000), the Tso Morari nappe migrated

parallel to the surface of underthrusting to a near-surface position below the earlier accreted and structurally higher Tetraogal and Mata nappes. During its emplacement as a SW-vergent nappe, the unit underwent Barrovian-type regional metamorphism, which affected the entire North Himalayan nappe stack under amphibolite-facies conditions at *c*. 47 Ma (De Sigoyer *et al*. 2000).

The Tetraogal nappe and Karzok Complex

The Tetraogal nappe (Steck *et al*. 1998) is principally made of Permo-Mesozoic sediments metamorphosed under epidote–amphibolite-facies conditions. This tectonic unit may be considered as a basal slice of the higher Mata nappe. Between these two nappes, along the thrust between the Mata and Tetraogal nappes, lies the 300 m thick mafic and ultramafic Karzok Complex (Berthelsen 1953). As the tectonometamorphic history of the smaller Tetraogal nappe and Karzok Complex is similar to that of the larger Mata nappe, we will not consider them any further.

The Mata nappe

Stratigraphic relationships show that the Mata nappe follows a recumbent fold structure characterized by a normal and an inverted fold limb (Fig. 3; Steck *et al*. 1998). The Ordovician Rupshu granite–gneiss (Girard & Bussy 1999) represents the core of this SW-vergent fold nappe and is surrounded by Precambrian to Liassic sediments. The Rupshu granite is contemporaneous with the nearby Nyimaling granite, which lies in a similar structural setting (Stutz & Thöni 1987). The core was deformed under epidote–amphibolite-facies metamorphic conditions, whereas the frontal part is characterized by a non-metamorphic brittle imbricate thrust (Girard *et al*. 1999).

Sampling and analytical procedures

Twenty-five samples, each weighing 5–15 kg, were collected for fission-track analyses. Apatite and zircon concentrates were obtained by crushing and standard heavy liquid and magnetic separation techniques. Mounting, polishing and etching were carried out following standard procedure of the London Fission Track Research Group (apatite etching with 5N HNO_3 at 20 °C for 20 s, and zircon etching with KOH–NaOH at 220 °C for between 12 and 36 h). Mounts were irradiated with muscovite external detectors and dosimeter glass CN-5 for apatite, and CN-2 for zircon at the thermal neutron facility of the Risø reactor, Denmark. Fission-track densities were measured using an optical microscope at 1250× magnification with an oil objective. Ages ($\pm 1\sigma$) were calibrated by the zeta method (Hurford & Green 1983), using a zeta factor of 339 ± 5 for apatite, and of 125 ± 5 for zircon determined by multiple analyses of apatite and zircon standards following the recommendations of Hurford (1990).

For $^{40}Ar/^{39}Ar$ dating, 10 samples (biotite, phengite, hornblende) were chosen, when possible using the same samples as for FT dating. The analytical procedure is similar to that described by Cosca *et al*. (1998).

Results

Fission-track results were obtained for 17 apatite and 16 zircon samples (Figs 2 and 3, Tables 2 and 3). Uranium inhomogeneity, inclusions, small grain size and quantity of mineral separate combined to prevent analysis of the remaining samples. For the $^{40}Ar/^{39}Ar$ method, only five samples yielded results that could be interpreted with high degrees of confidence for reconstructing the geological history (Fig. 4, Table 4). Most samples gave complicated age spectra as a result of either the occurrence of several generations of the same mineral phase or post-crystallization redistribution of argon within the grains. All samples are at held at the Mineralogy Institute of Lausanne.

The Ladakh Batholith

A granite sample from the Ladakh Batholith (sample A), corresponding to a phase III pluton of Sharma (1991), yields hornblende and biotite $^{40}Ar/^{39}Ar$ plateau ages of 44.7 ± 0.3 Ma and 32.6 ± 0.2 Ma, respectively. An apatite FT central age for this sample is 5 ± 1 Ma, with a long mean track length of 14.73 ± 0.14 μm, which is diagnostic of rapid cooling through the Partial Annealing Zone (PAZ, 60–110 °C).

The Indus and Chulze molasses

About 5 km SE of the granite, a sandstone from the Indus Molasse (sample B) has a zircon FT age of 23 ± 2 Ma and an apatite FT age of 7 ± 2 Ma with a long mean track length (14.62 ± 0.33 μm). A sandstone (sample D) from the Chulze Molasse yields a zircon FT age of 40 ± 2 Ma and an apatite FT age of 6 ± 2 Ma (uranium inhomogeneity in the grains prevented measure of the mean track length).

The Indus Suture Zone

Only a few zircon grains separated from a pegmatitic gabbro sample from the Nidar ophiolite were obtained for this zone, and the poor quality of these grains produced an imprecise average age of 88 ± 16 Ma.

The Tso Morari nappe

In this unit, apatite FT ages show a well-developed correlation with respect to their position away from the Ribil–Zildat Fault (Fig. 3). The youngest age, 7.5 ± 1.5 Ma, which also has the longest mean track length (15.22 ± 0.25 μm), is found in the Zildat Valley a few hundred metres south of the Ribil–Zildat Fault (sample E). In contrast, in the southern part of the nappe, apatite ages range from 21 ± 3 to 26 ± 3 Ma (samples J, K and L). These ages have slightly shorter mean track lengths of between 14.52 ± 0.2 μm and 13.52 ± 0.16 μm (Fig. 5). Zircon FT ages are between 34 ± 2 Ma and 45 ± 2 Ma and show no correlation with the structural position of the samples. Only two samples from the Tso Morari nappe yielded readily interpretable $^{40}Ar/^{39}Ar$ ages (Fig. 4). One sample of phengite yielded a $^{40}Ar/^{39}Ar$ plateau age of 53.8 ± 0.2 Ma (sample E), and a biotite yielded a near-plateau age of 51.1 ± 0.1 Ma (sample H).

The Mata nappe

In the Mata nappe, zircon FT ages range from 36 ± 2 Ma to 45 ± 2 Ma, similar to zircon FT ages from the Tso Morari nappe, and show no relation to their structural position. Apatite FT ages are generally older than apatite ages from the Tso Morari unit, with a maximum age of 40 ± 1 Ma obtained in the core of the Rupshu granite. Two samples (O and P), collected from the Ruphsu granite between Tso Morari Lake at 4550 m and Mt Mata at 6250 m, have within 1σ error broadly the same age (36 ± 2.5 and 40 ± 0.3 Ma) and mean track lengths (14.23 ± 0.12 μm and 14.54 ± 0.22 μm). A few kilometres south of this

Table 2. *Apatite and zircon fission-track analytical results*

Sample number	Location Lat. °N/Long. °E	Elevation (m)	Rock type Formation, unit	Apatite central age (Ma) ±1σ	Apatite mean track length (μm)	SD (μm)	Zircon central age (Ma) ±1σ
A	Chumatang 33°22′26.3′/078°21′18.6′	4150	Granite Ladakh Batholith	5.2 ± 0.5 (20)	14.73 ± 0.14 (75)	1.18	
B	Chumatang 33°19′31.6′/078°23′31.0′	4150	Sandstone Indus Molasse	7.4 ± 0.7 (20)	14.62 ± 0.33 (21)	1.49	23 ± 2 (3)
C	Raldong 33°15′18.3′/078°26′22.3′	4200	Metagabbro Indus Suture Zone				88 ± 16 (6)
D	Drakkarpo 33°15′19.6′/078°23′59.6′	4300	Sandstone Indus Molasse	6.1 ± 1.5 (7)			40.5 ± 2.1 (16)
E	Zildat Phu 33°14′34.8′/078°21′16.4′	4600	Gneiss Tso Morari gneiss	7.5 ± 1.5 (19)	15.22 ± 0.25 (13)	0.86	45 ± 2 (21)
F	Kiagar La 33°10′00.3′/078°21′37.0′	4750	Granite Tso Morari gneiss	7.6 ± 0.8 (6)	15.08 ± 0.34 (19)	1.45	38 ± 2 (18)
G	Polokongka La	4900	Granite Tso Morari gneiss				34 ± 2 (16)
H	Pera 33°07′16.4′/078°20′12.7′	4800	Orthogneiss Tso Morari gneiss	13.2 ± 0.8 (20)	14.23 ± 0.21 (74)	1.79	36 ± 2 (9)
I	Kiagar Tso 33°05′31.2′/078°17′20.9′	4800	Orthogneiss Tso Morari gneiss	16.4 ± 0.7 (20)	14.28 ± 0.12 (100)	1.2	37 ± 3 (11)
J	Gyanbarma		Orthogneiss Tso Morari gneiss	25.7 ± 2.6 (20)	14.52 ± 0.2 (19)	0.85	40 ± 2 (11)
K	Peldo 32°59′52.5′/078°15′37.8′	4600	Orthogneiss Tso Morari gneiss	23.4 ± 1.1 (20)	13.52 ± 0.16 (101)	1.62	35 ± 2 (17)
L	Tetraogal La 32°59′36.6′/078°15′21.4′	4850	Micaschist Precambrian–Cambrian, TM	21.5 ± 3.3 (10)			
M	Zerlung Marlung 32°55′52.7′/078°15′10.6′	4900	Metagraywacke Precambrian–Cambrian, Mata	30.5 ± 2.1 (17)	13.93 ± 0.15 (51)	1.09	38 ± 4 (7)
N	Kherlung 32°54′15.5′/078°15′10.6′	5450	Orthogneiss Rupshu granite, Mata				45 ± 7 (7)
O	Mt Mata 32°53′45.0′/078°13′46.3′	6100	Granite Rupshu granite, Mata	36.0 ± 2.5 (22)	14.23 ± 0.12 (73)	0.99	37 ± 2 (17)
P	Kherlung 32°53′07.5′/078°16′28.8′	4700	Granite Rupshu granite, Mata	39.9 ± 0.3 (26)	14.54 ± 0.22 (38)	1.36	45 ± 2 (23)
Q	Kele	4700	Granite Rupshu granite, Mata	14.1 ± 1.1 (20)	13.49 ± 0.15 (106)	1.55	
R	Kore Misikle	4700	Orthogneiss Rupshu granite, Mata	29.5 ± 2.8 (20)	14.35 ± 0.30 (13)	1.04	42 ± 3 (15)
S	Kele 32°49′15.4′/078°16′51.9′	4800	Metapelite Precambrian–Cambrian, Mata	20.1 ± 2.5 (11)			
T	Kiangdom 32°45′30.3′/078°18′36.2′	4700	Metapelite Precambrian–Cambrian, Mata	15.3 ± 1.2 (18)	14.23 ± 0.22 (40)	1.38	36 ± 2 (12)
U	Tso Kar Sample from De Sigoyer *et al*. (2000)		Metapelite Tso Morari gneiss	11.5 ± 1.8 (20)			
V	Nuruchan Sample from De Sigoyer *et al*. (2000)		Metapelite Tso Morari gneiss	14.1 ± 1.3 (20)			

Samples correspond to the letters in the map in Fig. 2. Central age is a modal age, weighted for different precisions of individual crystals. Parentheses show number of grains counted for age determination and number of tracks used for length measurement. The precision on the track length is the standard error ($\pm 1\sigma$; $\sigma = SD/\sqrt{n}$) and SD corresponds to the deviation of the track-length distribution. Analyses were carried out by external method using 0.5 for the $4\pi/2\pi$ geometry correction factor. Ages were calculated using $\zeta_{CN5} = 339 \pm 5$ and $\zeta_{CN2} = 125 \pm 5$ calibrated using IUGS apatite and zircon age standards, respectively; analyst: Andrew Carter.

locality, also in the Rupshu granite, apatite yields an age of 14 ± 1 Ma (sample Q) with moderately long mean track length of 13.49 ± 0.15 μm. In the Mata nappe the youngest apatite ages have the shortest mean track length (Fig. 5), in contrast to the relationship observed in the Tso Morari unit.

$^{40}Ar/^{39}Ar$ mica ages for most samples give highly discordant internal age spectra, except for one sample of biotite with an age of 457 ± 2 Ma obtained in the Rupshu granite (Fig. 4; sample P).

Interpretation

Samples collected at outcrop today yield differences in measured FT age and track length that reflect the exhumation paths of samples from different crustal depths at different rates, providing a series of records, each recording a different part of the overall regional history. In this study, there is no clear relationship between sample elevation and FT age (although the second oldest age is found at the highest elevation (sample O) and the youngest

Table 3. *Supplemental data for apatite and zircon fission-track analytical results*

Sample number		Apatite						Zircon					
This paper	Personal	Dosimeter	Spontaneous	Induced	Age dispersion		Central age	Dosimeter	Spontaneous	Induced	Age dispersion		Central age
		ρ_d	ρ_s	ρ_i	$P(\chi^2)$	RE%	(Ma) ± 1σ	ρ_d	ρ_s	ρ_i	$P(\chi^2)$	RE%	(Ma) ± 1σ
A	MS798	1.137	0.083	3.035	90	0	5.2 ± 0.5						
		(3274)	(140)	(5140)			(20)						
B	MS1198	1.14	0.125	3.258	85	0	7.4 ± 0.7	4.164	2.139	2.461	80	0	23 ± 2
		(3274)	(116)	(3021)			(20)	(2847)	(166)	(191)			(3)
C	MS1498							4.158	2.855	0.834	<1	38.6	88 ± 16
								(2847)	(558)	(163)			(6)
D	MS1798	1.298	0.06	2.161	60	0	6.1 ± 1.5	0.362	5.695	3.224	30	0.4	40.5 ± 2.1
		(7196)	(18)	(647)			(7)	(2550)	(1263)	(715)			(16)
E	MS2498	1.153	0.013	0.339	80	0	7.5 ± 1.5	0.518	7.528	5.454			45 ± 2
		(3274)	(27)	(700)			(19)	(3364)	(2817)	(2041)			(21)
F	MS2898	1.159	0.157	4.056	80	0	7.6 ± 0.8	4.155	5.598	3.843	30	8.4	38 ± 2
		(3274)	(102)	(2642)			(6)	(2847)	(2064)	(1417)			(18)
G	AS9660							4.121	6.454	4.89	<1	16.7	34 ± 2
								(2847)	(2138)	(1620)			(16)
H	MS3398	1.164	0.331	4.969	10	13.5	13.2 ± 0.8	4.155	5.807	4.166	75	0.3	36 ± 2
		(3274)	(551)	(8250)			(20)	(2847)	(998)	(716)			(9)
I	MS3498	1.17	0.663	7.968	90	0	16.4 ± 0.7	4.153	7.109	5.056	<1	18.6	37 ± 3
		(3274)	(808)	(9719)			(20)	(2847)	(1340)	(953)			(11)
J	G9628	1.225	0.208	1.672	15	21.9	25.7 ± 2.6	4.121	6.96	4.532	<1	12.9	40 ± 2
		(3274)	(146)	(1175)			(20)	(2847)	(1476)	(961)			(11)
K	MS4098	1.181	0.543	4.622	20	3.2	23.4 ± 1.1	4.15	4.735	3.419	7	11.8	35 ± 2
		(3274)	(641)	(5458)			(20)	(2847)	(1608)	(1161)			(17)
L	MS4198	1.235	0.382	0.369	90	0	21.5 ± 3.3						
		(6849)	(46)	(446)			(10)						
M	MS5698	1.203	0.357	2.381	85	0	30.5 ± 2.1	4.138	4.702	3.039	<1	23.6	38 ± 4
		(3274)	(263)	(1752)			(17)	(2847)	(958)	(619)			(7)
N	MS5298							4.144	8.35	4.919	<1	42.5	45 ± 7
								(2847)	(949)	(559)			(7)
O	MS5598	1.198	0.258	1.454	30	10.2	36.0 ± 2.5	4.141	6.848	4.839	2	13.5	37 ± 2
		(3274)	(301)	(1695)			(22)	(2847)	(1585)	(1120)			(17)
P	MS5898	1.209	0.359	1.832	60	0.3	39.9 ± 0.3	4.135	7.303	4.171	<1	10.8	45 ± 2
		(3274)	(344)	(1752)			(26)	(2847)	(2824)	(1613)			(23)
Q	V9692	1.22	0.161	2.364	15	15.6	14.1 ± 1.1						
		(3274)	(225)	(3296)			(20)						
R	MS6898	1.214	0.122	0.85	60	5.7	29.5 ± 2.8	4.138	5.303	3.219	<1	17.9	42 ± 3
		(3274)	(133)	(925)			(20)	(2847)	(2036)	(1236)			(15)
S	MS6398	1.235	0.262	2.692	<1	24.5	20.1 ± 2.5						
		(6849)	(150)	(1541)			(11)						
T	MS6498	1.235	0.168	2.283	70	8.9	15.3 ± 1.2	0.509	6.556	5.829			36 ± 2
		(6849)	(213)	(2892)			(18)	(3364)	(1137)	(1220)			(12)
U	LK9340	1.181	0.083	1.439	65	0	11.5 ± 1.8						
		(6548)	(46)	(798)			(20)						
V	LK9342	1.181	0.104	1.502	10	15.7	14.1 ± 1.3						
		(6548)	(156)	(2248)			(20)						

Samples correspond to the letter in the map in Fig. 2. ρ, track density ($\times 10^6$ tracks cm^{-2}); subscripts d, s and i denote, respectively, tracks in the fluence monitor glass, spontaneous tracks and induced tracks. Parentheses show number of grains counted for age determination and number of tracks used for length measurement. $P(\chi^2)$ is the probability for obtaining χ^2 value for ν degrees of freedom, where ν = numbersofcrystals − 1 (Galbraith 1981). RE% corresponds to the relative error of the central age. Central age is a modal age, weighted for different precisions of individual crystals. Analyses were carried out by external method using 0.5 for the $4\pi/2\pi$ geometry correction factor. Ages were calculated using $\zeta_{CN5} = 339 \pm 5$ and $\zeta_{CN2} = 125 \pm 5$ calibrated using IUGS apatite and zircon age standards, respectively; analyst: Andrew Carter.

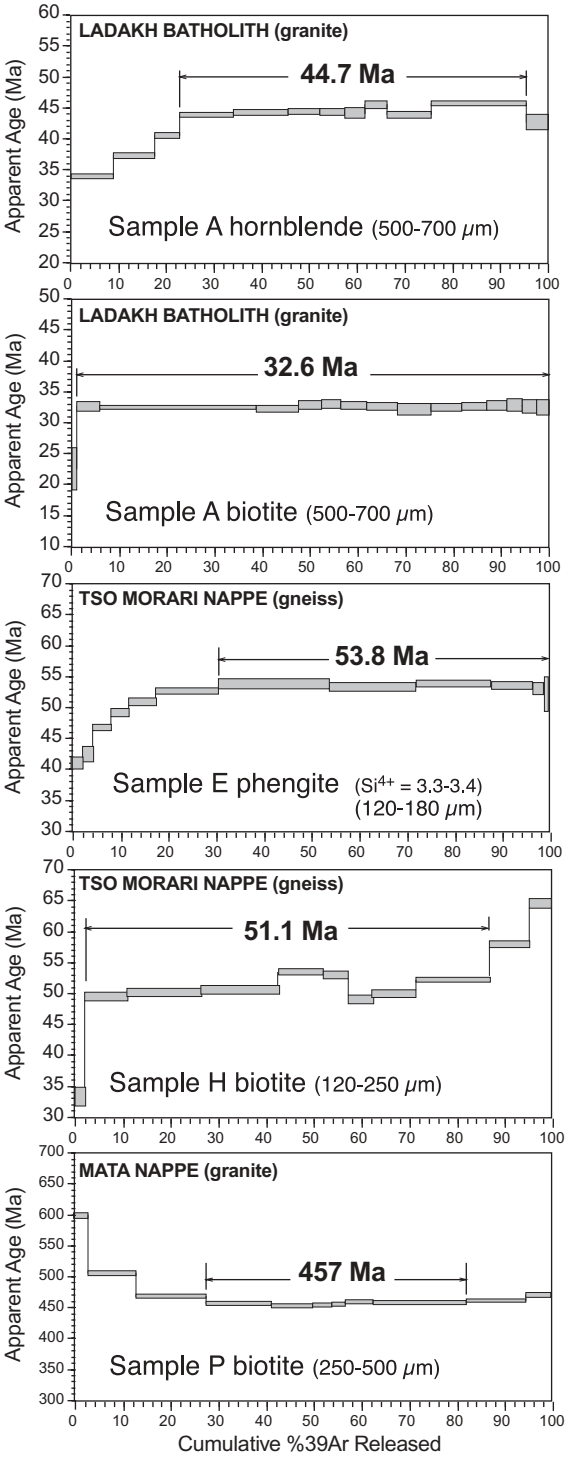

Fig. 4. $^{40}Ar/^{39}Ar$ age spectra with plateau ages indicated (except for sample H, which yields a near-plateau age).

age at lowest elevation (Figs 2 and 3; sample A), but more interestingly there is wide variation in FT age across the region. If exhumation had occurred uniformly we would expect to find similar ages at similar elevations. As we do not, the region must have experienced a variable exhumation history and therefore we need to consider the relationships between sample location, lithology and related structures. First we shall consider results from units located north of the Ribil–Zildat Fault and then focus on interpretation of samples located to the south, from the Mata and Tso Morari nappes.

Crystallization and cooling of the Ladakh Batholith

Given that argon is retained in amphiboles at relatively high temperatures (e.g. McDougall & Harrison 1988), the 44.7 ± 0.3 Ma $^{40}Ar/^{39}Ar$ hornblende age from a granite sample of the Ladakh Batholith should represent a time near its crystallization. This age is consistent with crystallization of the igneous rocks before *c*. 45 Ma and is hence broadly coeval with the magmatic activity responsible for the Leh pluton, which is estimated at 49.8 ± 0.8 Ma on the basis of U/Pb on zircon (Weinberg & Dunlap 2000; for all cited ages, also refer to Table 1). The younger $^{40}Ar/^{39}Ar$ biotite and apatite FT ages record continuing cooling below *c*. 320 °C and *c*. 100 °C, respectively. A plot of time and temperature for this granite based on the $^{40}Ar/^{39}Ar$ and apatite FT results shows at first sight little evidence for any significant change in long-term cooling rate (Fig. 6). However, the apatite FT cooling age of the Ladakh Batholith from the present study, like those from Sharma & Choubey (1983), is much younger compared with the 28 ± 3 Ma ages measured at Upshi, *c*. 100 km west of this transect (Sinclair & Jaffey 2001). In the central part of the batholith about 70 km NW of Chumatang, Dunlap *et al*. (1998) also estimated from a $^{40}Ar/^{39}Ar$ K-feldspar modelled age that the batholith already cooled to 150 °C at 36 Ma. Therefore the much younger cooling ages from Chumatang may be explained by a longer stay of this part of the batholith at greater depth owing to its local overthrusting by the molasse during Late Eocene time.

Formation and cooling of the Indus and Chulze molasses

The zircon FT age of 23 ± 2 Ma from a non-metamorphosed sandstone of the Indus Molasse is older than its sedimentation. This age is interpreted as a cooling age of the detrital source, which most probably is the adjacent Ladakh Batholith. The nearness of the sandstone outcrop to the batholith (about 2 km), the occurrence of K-feldspar and abundance of quartz, and the absence of any Fe–Mg minerals such as pyroxene or olivine that come from the Indus Suture Zone, suggest that this late-deposited molasse is the erosion product of the batholith. Indeed, Garzanti & Van Haver (1988) also observed that most of post-Eocene sediments were made of detritus from granitoid rocks. The 7.4 ± 0.7 Ma apatite FT age is related to cooling of the molasse following its burial (Fig. 6).

In the Chulze Molasse, a well-constrained zircon FT age (41 ± 2 Ma) is older than the sandstone deposition as a peak temperature of *c*. 250 °C during its burial was not high enough to anneal the fission tracks in zircon. The relative error of the central age is small (0.4%), suggesting that the origin of these zircons is a single source, probably the already emplaced North Himalayan nappe stack (see below). Indeed, De Sigoyer (1998) proposed that this molasse is the erosional product of the Oligocene relief formed during the thickening of the crust. The apatite FT age (6 ± 2 Ma) is similar to those measured in adjacent units and therefore suggests that the area lying between the Ribil–Zildat Fault and the central part of Ladakh Batholith cooled through the apatite PAZ during Late Miocene time.

Metamorphism of the Indus Suture Zone

The unexpected old zircon FT age (88 ± 16 Ma) from the Nidar ophiolite could be related to cooling following low-grade

Table 4. *Ar analytical data from furnace incremental heating experiment*

T (°C)	^{40}Ar (10^{-15} mol)	^{39}Ar (10^{-16} mol)	^{38}Ar (10^{-18} mol)	^{37}Ar (10^{-16} mol)	^{36}Ar (10^{-18} mol)	^{39}Ar (% of total)	^{40}Ar (%)	Age ± 2σ (Ma)
Sample A (MS798), hornblende, Ladakh Batholite (granite)								
850	30.50 ± 0.02	57.91 ± 0.06	17.78 ± 0.87	12.93 ± 0.19	19.81 ± 0.22	8.7	80.8	34.58 ± 0.26
950	31.04 ± 0.03	57.18 ± 0.09	23.27 ± 5.20	93.58 ± 0.39	17.10 ± 0.27	8.6	85.9	38.00 ± 0.29
975	19.27 ± 0.02	33.81 ± 0.03	16.09 ± 3.20	80.75 ± 0.28	9.33 ± 0.22	5.1	88.8	41.34 ± 0.32
1000	44.69 ± 0.03	74.06 ± 0.11	39.91 ± 5.66	302.33 ± 0.54	22.52 ± 0.28	11.1	90.3	44.74 ± 0.32
1020	44.75 ± 0.08	75.35 ± 0.09	45.21 ± 5.39	324.95 ± 0.62	19.91 ± 0.25	11.3	92.4	45.10 ± 0.32
1030	26.27 ± 0.02	44.10 ± 0.05	48.37 ± 1.86	185.92 ± 0.42	11.62 ± 0.23	6.6	92.4	45.21 ± 0.33
1040	20.01 ± 0.02	33.79 ± 0.03	23.60 ± 3.23	142.67 ± 0.42	8.50 ± 0.22	5.1	92.9	45.20 ± 0.35
1050	16.23 ± 0.09	27.35 ± 0.14	25.31 ± 2.66	114.58 ± 0.51	7.17 ± 0.21	4.1	92.3	45.03 ± 0.52
1060	3.52 ± 0.01	4.81 ± 0.01	3.96 ± 0.71	17.77 ± 0.17	3.19 ± 0.15	0.7	76.9	46.23 ± 0.87
1075	18.58 ± 0.03	30.88 ± 0.07	26.84 ± 1.86	140.03 ± 0.49	7.59 ± 0.21	4.6	93.7	46.38 ± 0.38
1100	36.01 ± 0.13	61.41 ± 0.12	32.14 ± 5.11	292.20 ± 0.67	16.48 ± 0.24	9.2	92.7	44.74 ± 0.37
1150	77.70 ± 0.10	132.48 ± 0.23	49.36 ± 12.15	671.67 ± 1.76	26.75 ± 0.29	19.9	96.5	46.61 ± 0.33
1200	18.23 ± 0.20	31.57 ± 0.16	22.91 ± 3.45	151.40 ± 0.91	9.15 ± 0.24	4.7	91.5	43.52 ± 0.68
Weight 21.89 mg					Plateau age (700–1100 °C) 44.7 ± 0.3 Ma			
J value 0.00461					Integrated age 42.8 ± 0.2 Ma			
Sample A (MS798), biotite, Ladakh Batholite (granite)								
600	78.61 ± 0.88	54.99 ± 0.27	10.46 ± 2.72	2.49 ± 2.84	214.29 ± 1.14	1.1	19	22.35 ± 1.70
700	135.69 ± 0.94	240.59 ± 0.62	61.92 ± 21.43	2.35 ± 2.96	133.12 ± 1.04	4.8	70.6	32.37 ± 0.43
800	674.19 ± 1.52	1638.36 ± 1.89	418.11 ± 41.52	5.38 ± 2.91	70.80 ± 0.92	32.9	96.8	32.23 ± 0.23
825	178.79 ± 1.06	445.68 ± 2.17	115.97 ± 3.99	3.13 ± 2.86	7.86 ± 0.86	8.9	98.7	32.00 ± 0.33
850	96.99 ± 0.87	236.53 ± 0.37	44.76 ± 18.42	3.24 ± 2.80	5.95 ± 0.84	4.7	98.2	32.55 ± 0.38
875	84.40 ± 0.84	204.28 ± 0.31	46.51 ± 2.69	2.91 ± 2.76	5.68 ± 0.83	4.1	98	32.74 ± 0.41
900	111.52 ± 0.87	269.93 ± 0.59	41.98 ± 2.98	3.76 ± 2.74	9.24 ± 0.82	5.4	97.5	32.58 ± 0.35
925	128.81 ± 0.91	316.57 ± 1.05	55.19 ± 5.11	4.03 ± 2.73	7.12 ± 0.82	6.3	98.3	32.36 ± 0.34
950	142.01 ± 1.63	353.06 ± 2.59	94.37 ± 3.84	4.76 ± 2.73	9.32 ± 0.82	7.1	98	31.88 ± 0.49
975	129.60 ± 0.90	319.49 ± 0.78	38.91 ± 4.55	5.18 ± 2.75	7.61 ± 0.81	6.4	98.2	32.22 ± 0.33
1000	106.10 ± 0.86	260.56 ± 0.34	30.53 ± 3.41	5.26 ± 2.79	5.70 ± 0.81	5.2	98.4	32.40 ± 0.35
1025	84.86 ± 0.87	207.53 ± 0.35	36.42 ± 14.16	4.81 ± 2.85	5.16 ± 0.80	4.2	98.2	32.47 ± 0.42
1050	64.46 ± 0.89	158.14 ± 0.27	32.41 ± 13.03	5.50 ± 2.92	2.69 ± 0.81	3.2	98.8	32.56 ± 0.52
1075	59.34 ± 0.91	146.98 ± 0.27	39.70 ± 13.22	6.19 ± 3.02	2.02 ± 0.81	2.9	99	32.33 ± 0.57
1100	53.94 ± 0.95	134.61 ± 0.35	30.26 ± 1.87	10.54 ± 3.13	0.99 ± 0.82	2.7	99.6	32.27 ± 0.64
Weight 21.83 mg					Plateau age (700–1100 °C) 32.57 ± 0.19 Ma			
J value 0.00461					Integrated age 32.46 ± 0.19 Ma			
Sample E (MS2498), phengite, Tso Morari nappe (gneiss)								
700	708.92 ± 1.67	1002.16 ± 0.84	1428.49 ± 14.63	1138.30 ± 31.04	780.02 ± 8.38	2.8	68.4	41.12 ± 0.43
750	617.32 ± 1.78	810.20 ± 0.44	1251.93 ± 40.52	378.85 ± 9.98	715.88 ± 8.47	2.2	65.9	42.58 ± 0.48
800	832.52 ± 1.67	1460.63 ± 0.84	1687.43 ± 11.45	190.59 ± 5.88	68.11 ± 8.25	4.0	97.7	46.99 ± 0.38
825	827.90 ± 1.73	1404.49 ± 1.06	1683.37 ± 21.47	102.29 ± 4.87	26.10 ± 8.26	3.9	99.2	49.28 ± 0.40
850	1307.38 ± 1.68	2108.24 ± 0.71	2578.47 ± 28.66	74.04 ± 4.15	96.96 ± 8.08	5.8	97.8	51.15 ± 0.39
875	3087.14 ± 2.03	4787.55 ± 3.17	5678.32 ± 36.34	50.19 ± 4.08	291.49 ± 7.90	13.2	97.2	52.84 ± 0.39
900	5445.61 ± 19.49	8316.70 ± 17.89	9674.94 ± 163.10	45.29 ± 4.35	421.52 ± 8.10	22.9	97.7	53.93 ± 0.45
925	4281.69 ± 4.51	6599.58 ± 5.96	8292.48 ± 36.16	35.86 ± 4.26	284.77 ± 7.82	18.1	98	53.61 ± 0.40
975	3762.66 ± 3.15	5715.09 ± 2.81	6803.68 ± 92.85	30.46 ± 4.19	360.96 ± 7.84	15.7	97.1	53.92 ± 0.40
1000	2048.28 ± 1.86	3152.07 ± 1.31	3768.48 ± 31.76	32.78 ± 4.06	130.42 ± 7.87	8.7	98.1	53.75 ± 0.40
1025	655.88 ± 1.81	1038.12 ± 0.67	1323.69 ± 77.18	30.39 ± 4.57	8.56 ± 8.40	2.9	99.7	53.07 ± 0.46
Weight 20.65 mg					Plateau age (900–1025 °C) 53.79 ± 0.13 Ma			

(*continued overleaf*)

Table 4. *continued*

T (°C)	^{40}Ar (10^{-15} mol)	^{39}Ar (10^{-16} mol)	^{38}Ar (10^{-18} mol)	^{37}Ar (10^{-16} mol)	^{36}Ar (10^{-18} mol)	^{39}Ar (% of total)	^{40}Ar (%)	Age ± 2σ (Ma)
J value 0.00480					Integrated age 52.5 ± 0.1 Ma			
Sample H (MS3398), biotite, Tso Morari nappe (gneiss)								
600	606.11 ± 1.94	715.60 ± 0.72	4076.00 ± 49.62	1175.67 ± 37.53	1129.16 ± 8.53	2.3	46.1	33.34 ± 0.55
700	2073.51 ± 1.70	2723.35 ± 1.67	16515.08 ± 26.93	643.91 ± 17.85	1616.80 ± 6.20	8.8	77.1	49.65 ± 0.39
750	3036.43 ± 5.71	4748.41 ± 5.91	27942.43 ± 342.69	246.33 ± 8.92	722.24 ± 6.32	15.3	93.1	50.22 ± 0.39
800	3065.78 ± 3.08	5016.45 ± 4.25	27962.67 ± 135.82	102.98 ± 6.42	197.13 ± 5.92	16.2	98.2	50.61 ± 0.37
850	1871.37 ± 1.96	2882.46 ± 2.12	14664.60 ± 317.99	63.04 ± 4.83	122.23 ± 5.92	9.3	98.2	53.74 ± 0.40
875	1044.46 ± 1.71	1643.70 ± 1.05	5675.66 ± 49.43	41.58 ± 4.59	32.19 ± 6.00	5.3	99.2	53.12 ± 0.41
900	929.74 ± 1.63	1590.14 ± 0.90	5285.43 ± 33.69	30.20 ± 4.52	16.38 ± 6.06	5.1	99.6	49.07 ± 0.38
950	1728.33 ± 1.89	2855.33 ± 1.54	12045.49 ± 123.43	30.17 ± 4.62	130.46 ± 6.03	9.2	97.8	49.94 ± 0.37
1000	2987.93 ± 2.87	4729.58 ± 2.67	25137.38 ± 136.06	21.83 ± 5.22	171.12 ± 6.19	15.2	98.4	52.41 ± 0.39
1050	1826.76 ± 1.97	2595.79 ± 0.95	12188.95 ± 94.51	27.75 ± 4.70	105.68 ± 6.55	8.4	98.4	58.34 ± 0.43
1100	1178.35 ± 2.02	1516.42 ± 1.19	4202.99 ± 12.99	47.33 ± 4.46	51.19 ± 6.90	4.9	98.8	64.64 ± 0.49
Weight 22.15 mg J value 0.00480					Forced Plateau age (700–1000 °C) 51.10 ± 0.09 Ma Integrated age 51.97 ± 0.08 Ma			
Sample P (MS5898), biotite, Mata nappe (granite)								
600	1684.53 ± 2.22	186.22 ± 0.37	489.04 ± 38.71	0.00 ± 0.00	221.65 ± 1.07	2.9	96.1	607.59 ± 3.56
700	4591.83 ± 4.32	639.18 ± 0.78	886.07 ± 35.84	0.73 ± 2.89	76.31 ± 1.04	10.1	99.5	513.40 ± 2.95
750	6100.94 ± 5.75	930.18 ± 0.67	1733.79 ± 51.62	1.91 ± 2.89	33.31 ± 1.06	14.7	99.8	475.44 ± 2.73
800	5527.16 ± 4.32	866.64 ± 0.57	752.92 ± 50.18	2.46 ± 2.84	20.80 ± 1.03	13.7	99.9	464.05 ± 2.66
850	3460.42 ± 3.04	546.89 ± 0.65	851.37 ± 40.14	2.79 ± 2.76	14.16 ± 0.91	8.6	99.9	460.78 ± 2.68
875	1656.24 ± 1.81	260.97 ± 0.33	528.11 ± 31.53	2.38 ± 2.72	8.35 ± 0.88	4.1	99.9	461.90 ± 2.70
900	1116.42 ± 0.96	175.35 ± 0.28	280.33 ± 22.91	2.58 ± 2.69	7.28 ± 0.85	2.8	99.8	463.04 ± 2.73
950	2343.84 ± 2.61	364.22 ± 0.39	602.69 ± 27.23	3.68 ± 2.68	23.89 ± 0.90	5.8	99.7	466.97 ± 2.72
1000	7933.50 ± 5.60	1240.10 ± 0.65	1463.61 ± 53.06	6.69 ± 2.74	45.52 ± 1.05	19.6	99.8	465.08 ± 2.66
1050	5083.22 ± 4.03	787.37 ± 0.68	784.07 ± 74.55	12.25 ± 2.88	28.64 ± 1.03	12.4	99.8	468.86 ± 2.69
1100	2169.42 ± 2.65	328.66 ± 0.46	605.83 ± 35.85	20.54 ± 3.05	15.12 ± 0.90	5.2	99.8	478.04 ± 2.81
Weight 23.79 mg J value 0.00461					Forced plateau age (800–1000 °C) 457 ± 2 Ma Integrated age 469 ± 2 Ma			

Data corrected for system blanks, radioactive decay subsequent to irradiation, mass discrimination and interfering K-, Ca- and Cl-derived isotopes of argon.

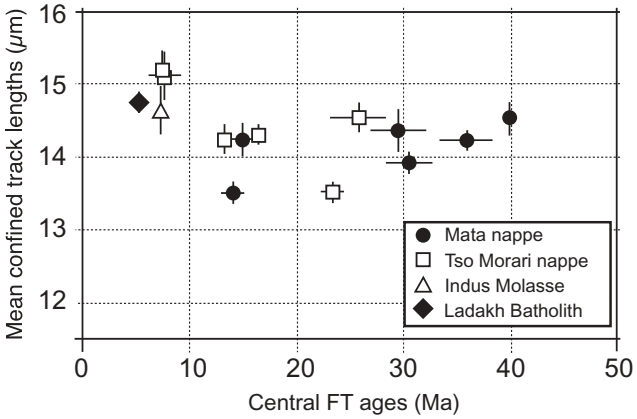

Fig. 5. Relationships between mean horizontal confined track lengths and fission-track ages. It should be noted that in the Tso Morari nappe, the longest mean track lengths are related to the youngest ages, and in the Mata nappe the longest mean track lengths are related to the oldest ages. Error bars correspond to the standard error of the mean for FT ages and lengths (not plotted when the symbol is larger than the error bar).

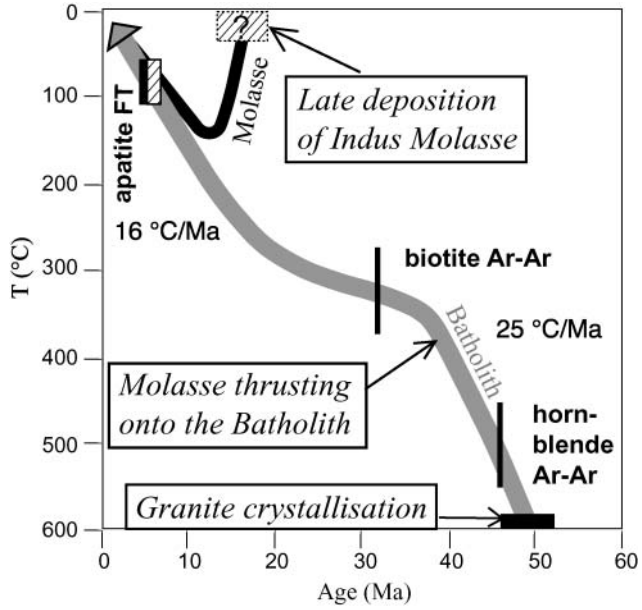

Fig. 6. Inferred *T–t* path for a phase III (Sharma 1991) granite of the Ladakh Batholith (sample A) and for a late deposition of the adjacent Indus Molasse (sample B). Sizes of the rectangles reflect the errors. Thrusting of the molasse onto the batholith could have perturbed the cooling history of the batholith during Eocene–Oligocene time; this period is suggested by K/Ar ages between 40 and 35 Ma for illites from the molasse (Van Haver *et al*. 1986).

metamorphism that affected the Indus Suture Zone long before continental collision. In the western part of the Indus Suture Zone, Maluski & Matte (1984) and Honegger *et al*. (1989) also reported Mid–Late Cretaceous ages for metamorphism that, however, has been related to high-pressure conditions.

Emplacement and metamorphism of the North Himalayan nappes

The $^{40}Ar/^{39}Ar$ ages of *c*. 54 Ma for phengite and *c*. 51 Ma for biotite from the Tso Morari nappe probably record cooling of the samples following amphibolite-facies metamorphism, and the phengite possibly records an earlier phase of the high-pressure metamorphism (see also De Sigoyer *et al*. 2000). In the Mata nappe, the *c*. 457 Ma $^{40}Ar/^{39}Ar$ biotite age in the Rupshu granite is simply a minimum age related to its cooling following emplacement of the pluton at 482.5 ± 1 Ma (Girard & Bussy 1999). No $^{40}Ar/^{39}Ar$ age has yet been obtained that would date the metamorphism in the Mata nappe.

The zircon FT ages of the Mata and Tso Morari nappes suggest that the whole region cooled through the 300–200 °C temperature range between 47 and 32 Ma. In the core of the Mata nappe, the small difference in age between zircon and apatite FT data (ages differ by <6–8 Ma for some samples) confirms that the two minerals record different periods of the same cooling event. These data are consistent with rapid exhumation of the Mata and Tso Morari nappes to a depth of some 10–15 km in the time interval between 45 and 40 Ma. This fast uplift initiated backfolding as a result of overthickening of the crust in the root zones of the nappes, and consequently created an early dome structure. The zircon FT ages indicate that the Mata nappe was emplaced and underwent Barrovian metamorphism before *c*. 45 Ma. This result is consistent with $^{40}Ar/^{39}Ar$ ages in the range of 42–45 Ma measured by Wiesmayr & Grasemann (1999) on illites related to the low-grade metamorphism observed in the frontal part of the nappe.

The 30 Ma age for greenschist-facies retrogression inferred from $^{40}Ar/^{39}Ar$ muscovite and biotite analyses by De Sigoyer *et al*. (2000) is younger than some of our zircon FT ages. However, this apparent contradiction is resolved when considering that De Sigoyer's samples were collected about 25 km to the west of the present transect, in a higher-grade zone that underwent amphibolite-facies metamorphic conditions (Fig. 2; kyanite–sillimanite–staurolite zone mapped by Girard (2001)). Consequently, De Sigoyer's samples cooled below the critical temperature for argon retention later than samples from the present study. The disagreement could also be partly due to a PAZ temperature range for zircon that is higher than the generally accepted values of 200–300 °C reported in the literature (Tagami *et al*. 1998). However, because the Mata nappe apatite and zircon FT data are similar in age, the latter explanation seems unlikely. We therefore suggest that greenschist-facies retrogression is older than *c*. 40 Ma for the central part of the Tso Morari nappe, but is *c*. 30 Ma old in the western part, which was located in the centre of a thermal dome.

Late exhumation of the North Himalayan nappes and brittle activity of the Ribil–Zildat Fault

Modelling the apatite FT ages and track length data provides additional insight into the low-temperature thermal history across the nappe. The root zone of the Tso Morari nappe, which is located close to the Ribil–Zildat Fault, underwent rapid cooling through *c*. 110–60 °C between 20 and 5 Ma. This equates to a minimum cooling rate of 15–20 °C Ma^{-1}, based on modelling of sample I (Fig. 7a); modelling of samples E, F and H yields higher cooling rates. At the Tso Morari nappe front, where the apatite FT ages are older, exhumation rates through the apatite PAZ appear marginally slower. For example, a gneiss sampled on the shore of Tso Morari Lake cooled at rates of $\leqslant 5$ °C Ma^{-1} (Fig. 7b). These results suggest that most of the Tso Morari nappe cooled since Late Eocene time at a fairly slow rate, except in the footwall of the Ribil–Zildat Fault, where late exhumation was significantly faster during Miocene brittle reactivation of the fault.

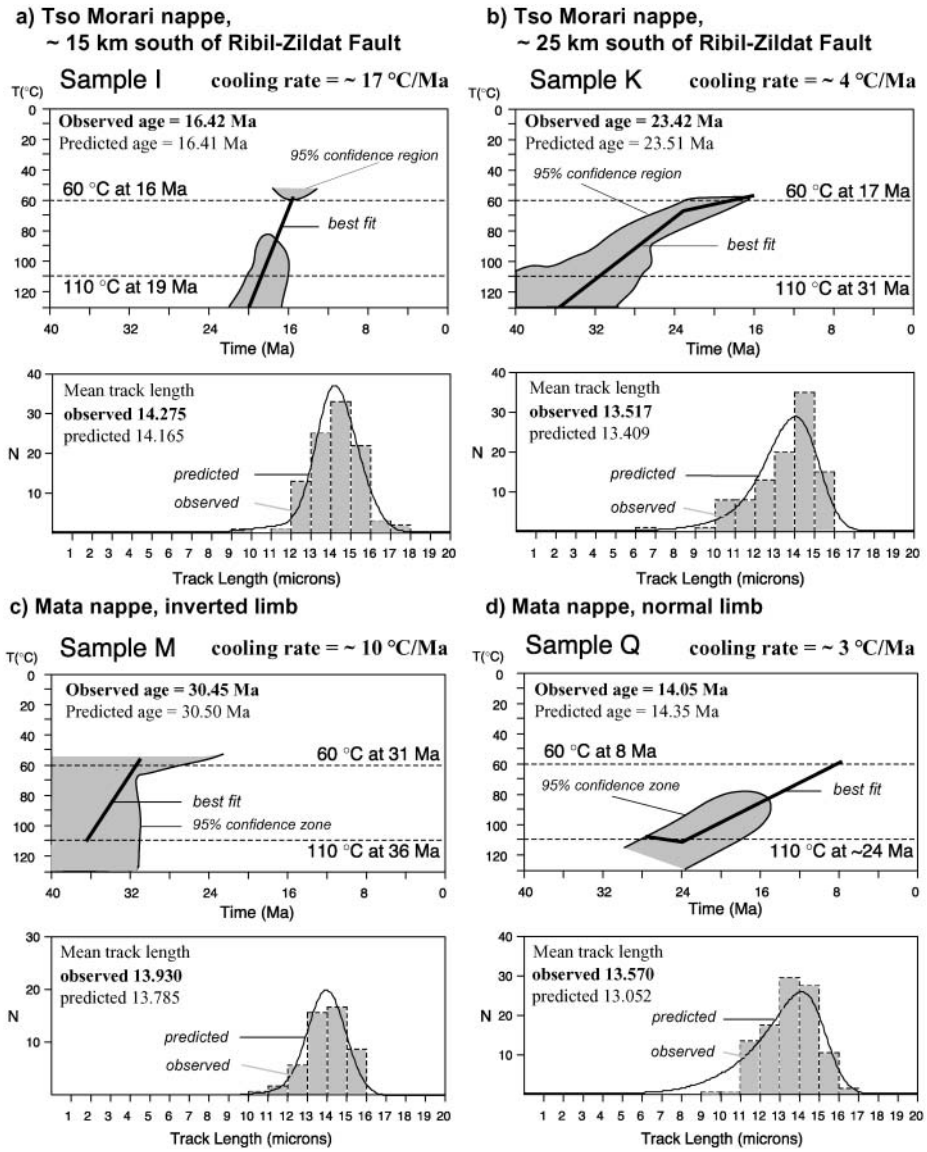

Fig. 7. In (**a**)–(**d**), the upper panels show thermal histories (bold line) of representative samples through the apatite PAZ; the lower panels show observed and predicted track length parameters, using the annealing model of Laslett & Galbraith (1996) based on Durango apatite.

In the Mata nappe, old and young FT ages occur at similar elevations and samples have similar variations in mean track length. No clear systematic relationship between sample FT parameters and location is observed, although the youngest ages occur in the southern part of the nappe. The youngest ages (samples Q, S and T) come from the upper part of the nappe in samples that originated from deeper crustal levels than the core of the Rupshu granite, which yields the oldest age (39.9 ± 0.3 Ma). The youngest age also has the shortest mean track length, indicating slower cooling through the apatite PAZ compared with the rest of the Mata nappe (Fig. 7c and d). Collectively, these data suggest that the Mata nappe experienced an early phase of rapid exhumation that terminated around 40–35 Ma, when the core of the nappe reached shallow structural levels (*c*. 3–5 km depth). Subsequent denudation has been moderately slow, except perhaps in the southern part of the nappe where an early dome folding phase and slightly faster denudation created a basin-type structure.

The slow cooling rates recorded in the Tso Morari and the Mata nappes since Late Eocene time are probably caused by the combination of weak tectonic activity and occurrence of dry climatic conditions.

Discussion and conclusions

Steck *et al*. (1998) and Girard (2001) presented a kinematic model to explain the tectonic evolution of the NW Himalaya along the Tso Morari–Spiti–Mandi transect. The new data presented here permit further refinement of this model (Fig. 8), as follows.

Around 55 Ma, during continental collision between India and Asia (Garzanti *et al*. 1987), the Tso Morari slab was subducted to a depth of at least 90 km where it underwent eclogite-facies metamorphism (De Sigoyer *et al*. 1997, 2000; Guillot *et al*. 1997; Mukherjee & Sachan 2001). Above the surface of underthrusting, the upper part of the Indian crust was sheared off and accreted, generating the Mata and Tetraogal nappes. Around the same time, compressive stress in the internal parts of the Indian margin generated the NE-vergent Shikar Beh nappe (Steck *et al*. 1993; Epard *et al*. 1995).

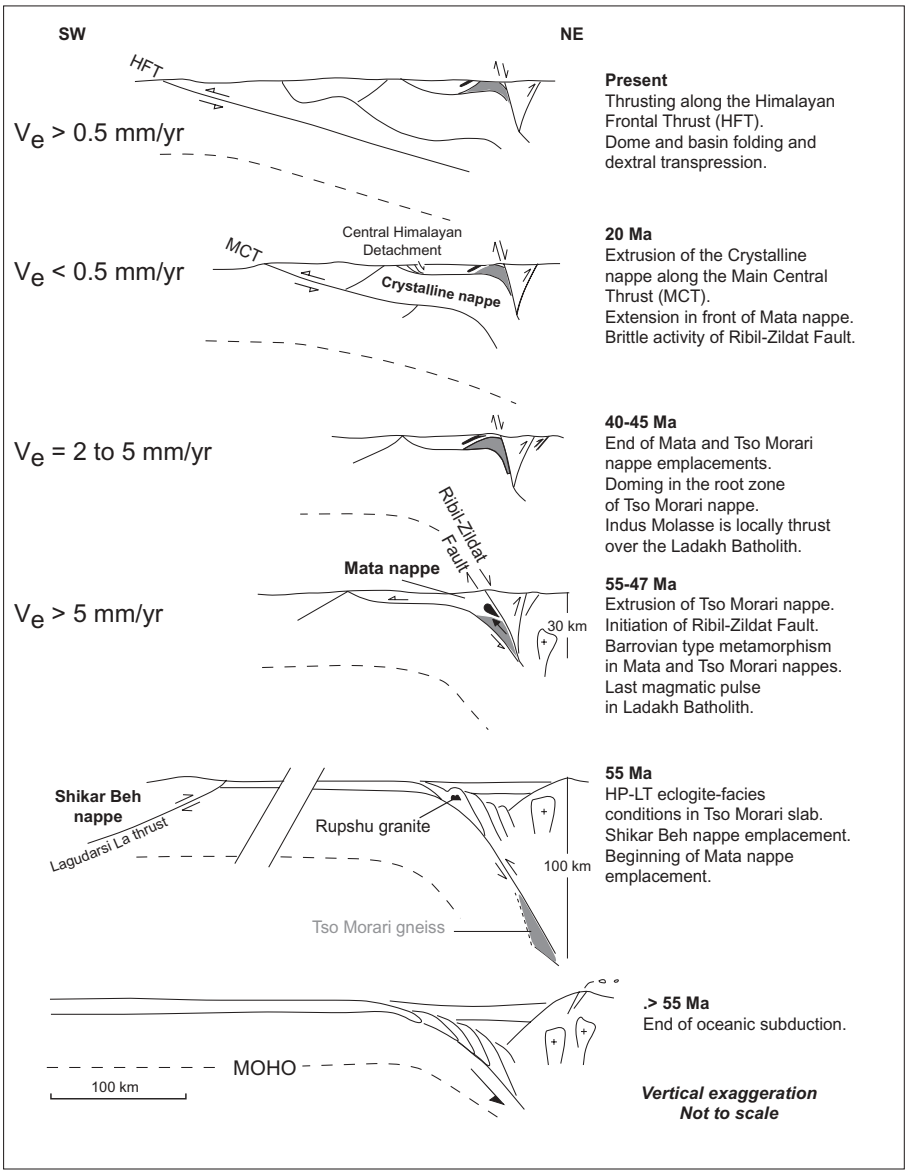

Fig. 8. Tectonic model for the Indus River–Tso Morari–Spiti–Mandi transect, modified from Steck *et al*. (1998) and Girard (2001). Ve, vertical exhumation rate for the root zone of Tso Morari nappe.

During early Eocene time, the Tso Morari slab was sheared off the subducted Indian crust and transported by buoyancy forces (Chemenda *et al*. 1995, 2000) toward the Earth's surface at a vertical exhumation rate of at least 5 mm a^{-1} (De Sigoyer *et al*. 2000). At *c*. 47 Ma the nappe stack was emplaced and the Tso Morari nappe was situated at a depth of *c*. 30 km (De Sigoyer *et al*. 2000; Girard 2001). Medium-pressure–high-temperature retrograde metamorphism occurred at this time, and was probably synchronous throughout the entire nappe stack. This is also the time of the last magmatic pulse in the Ladakh Batholith (Weinberg & Dunlap 2000).

By 45–40 Ma, fission-track data suggest that the entire nappe stack had been exhumed to a moderately shallow depth (*c*. 10 km). This implies fairly rapid vertical exhumation, estimated in the Tso Morari nappe to be 2–5 mm a^{-1}. This fast uplift initiated backfolding as a result of overthickening of the crust in the root zones of the nappes, and consequently created an early dome structure. The exhumation of the Tso Morari gneiss dome is therefore *c*. 20 Ma older than the exhumation of the Kangmar gneiss dome situated in the eastern part of the Himalayan belt (Chen *et al*. 1990; Guillot *et al*. 1998). Also during Late Eocene time, the Indus Molasse was locally thrust over the Ladakh Batholith.

Between 40 and 20 Ma, there was little tectonic activity in the North Himalayan nappe stack and dry climatic conditions probably appeared. Overall exhumation rates declined during this period.

At *c*. 20 Ma, the root zones of the nappe stack experienced increased exhumation linked to brittle reactivation of the Ribil–Zildat Fault. The North Himalayan nappe stack experienced extension, and in its frontal parts the Central Himalayan Detachment Zone (also know as the South Tibetan Detachment Zone; Burchfield & Royden 1985) developed between 22 and 19 Ma (Dèzes *et al*. 1999). Extension was coincident with extrusion of the Crystalline nappe along the Main Central Thrust at 23–17 Ma (Frank *et al*. 1977; Hubbard & Harrison 1989; White *et al*. 2002; Schlup 2003).

At present, late dome and basin structures are active with

wavelengths of 50–150 km and amplitudes of several thousands of metres. North-striking normal faults that form an angle of 45° with the Indus Suture, such as the Tso Morari Fault, are related to regional dextral transpression. Thrust activity has been transferred to the south along the Himalayan Frontal Thrust.

We gratefully acknowledge the Swiss National Science Foundation (grants 20-58777.99, to A.S.) for its financial support. M. Cellio, D. Giorgis, J. Hunziker, N. Kramar and J. Perrin are sincerely thanked for their scientific and psychological support during the field seasons. Special thanks go to the collaborators of the London Fission Track Research Group, especially to its director A. Hurford, who warmly collaborated with our Himalayan geological research programme. We are also grateful to R. Phillips and M. Thöni for their thorough and constructive reviews.

References

Berthelsen, A. 1953. On the geology of the Rupshu District, NW Himalaya; a contribution to the problem of the central gneisses. *Meddelelser fra Dansk Geologisk Forening*, **12**, 351–414.

Burchfield, B.C. & Royden, L.H. 1985. North–south extension within the convergent Himalayan region. *Geology*, **13**, 679–682.

Chemenda, A.I., Mattauer, M., Malavieille, J. & Bokun, A.N. 1995. A mechanism for syn-collisional rock exhumation and associated normal faulting: results from physical modelling. *Earth and Planetary Science Letters*, **132**, 225–232.

Chemenda, A.I., Burg, J.P. & Mattauer, M. 2000. Evolutionary model of the Himalaya–Tibet system: geopoem based on new modelling, geological and geophysical data. *Earth and Planetary Science Letters*, **174**, 397–409.

Chen, Z., Liu, Y., Hodges, K.V., Burchfiel, B.C., Royden, L.H. & Deng, C. 1990. The Kangmar dome: a metamorphic core complex in southern Xizang (Tibet). *Science*, **250**, 1552–1556.

Cosca, M.A., Mezger, K. & Essene, E.J. 1998. The Baltica–Laurentia connection: Sveconorwegian (Grenvillian) metamorphism, cooling, and unroofing in the Bamble Sector, Norway. *Journal of Geology*, **106**, 539–552.

De Sigoyer, J. 1998. *Mécanismes d'exhumation des roches de haute pression basse température en contexte de convergence continentale (Tso Morari, NO Himalaya)*. PhD thesis, Université Claude Bernard, Lyon.

De Sigoyer, J., Guillot, S., Lardeaux, J.-M. & Mascle, G. 1997. Glaucophane-bearing eclogites in the Tso Morari Dome (eastern Ladakh, NW Himalaya). *European Journal of Mineralogy*, **9**, 1073–1083.

De Sigoyer, J. & Chavagnac, V. *et al.*2000. Dating the Indian continental subduction and collisional thickening in the northwest Himalaya: multichronology of the Tso Morari eclogites. *Geology*, **28**, 487–490.

Dèzes, P.J., Vannay, J.-C., Steck, A., Bussy, F. & Cosca, M. 1999. Synorogenic extension; quantitative constraints on the age and displacement of the Zanskar Shear Zone (NW Himalaya). *Geological Society of America Bulletin*, **111**, 364–374.

Dunlap, W.J., Weinberg, R.F. & Searle, M.P. 1998. Karakoram fault zone rocks cool in two phases. *Journal of the Geological Society, London*, **155**, 903–912.

Epard, J.-L., Steck, A., Vannay, J.-C. & Hunziker, J. 1995. Tertiary Himalayan structures and metamorphism in the Kulu Valley (Mandi–Khoksar Transect of the western Himalaya); Shikar Beh Nappe and Crystalline Nappe. *Schweizerische Mineralogische und Petrographische Mitteilungen*, **75**, 59–84.

Frank, W., Thöni, M. & Purtscheller, F. 1977. Geology and petrography of Kulu–South Lahul area. *Colloques Internationaux du CNRS*, **268**, 147–160.

Frank, W., Graseman, B., Guntli, P. & Miller, C. 1995. Geological map of the Kishtwar–Chamba–Kulu region (NW, Himalaya, India). *Jahrbuch der Geologischen Bundesanstalt*, **138**, 299–308.

Fuchs, G. & Linner, M. 1996. On the geology of the suture zone and Tso Morari dome in Eastern Ladakh (Himalaya). *Jahrbuch der Geologischen Bundesanstalt*, **139**, 191–207.

Galbraith, R.F. 1981. On statistical models for fission track counts. *Mathematical Geology*, **13**, 471–478.

Gansser, A. 1964. *Geology of the Himalayas*. Wiley, Lonfon.

Garzanti, E. & Van Haver, T. 1988. The Indus clastics: forearc basin sedimentation in the Ladakh Himalaya (India). *Sedimentary Geology*, **59**, 237–249.

Garzanti, E., Baud, A. & Mascle, G. 1987. Sedimentary record of the northward flight of India and its collision with Eurasia (Ladakh Himalaya, India). *Geodinamica Acta*, **1**, 297–312.

Girard, M. 2001. *Metamorphism and Tectonics of the Transition between Non-metamorphic Tethyan Himalaya Sediments and the North Himalayan Crystalline Zone (Rupshu AreaLadakh, NW India)*. Mémoire de Géologie (Lausanne), **35**.

Girard, M. & Bussy, F. 1999. Late Pan-African magmatism in the Himalaya: new geochronological and geochemical data from the Ordovician Tso Morari metagranites (Ladakh, NW India). *Schweizerische Mineralogische und Petrographische Mitteilungen*, **79**, 399–418.

Girard, M., Steck, A. & Thélin, P. 1999. The Dutung–Thaktote extensional fault zone and nappe structures documented by illite crystallinity and clay-mineral paragenesis in the Tethys Himalaya between Spiti river and Tso Morari, NW India. *Schweizerische Mineralogische und Petrographische Mitteilungen*, **79**, 419–430.

Guillot, S., de Sigoyer, J., Lardeaux, J.-M. & Mascle, G. 1997. Eclogitic metasediments from the Tso Morari area (Ladakh, Himalaya): evidence for continental subduction during India–Asia convergence. *Contributions to Mineralogy and Petrology*, **128**, 197–212.

Guillot, S., Pochat, S., Zakarian, N. & Hodges, K.V. 1998. Evolution métamorphique du dôme de kangmar (Sud-Est-Xizang): implications pour les zones internes himalayennes. *Comptes Rendus de l'Académie des Sciences*, **327**, 577–582.

Guillot, S., Hattori, K.H. & de Sigoyer, J. 2000. Mantle wedge serpentinization and exhumation of eclogites: insights from eastern Ladakh, northwest Himalaya. *Geology*, **28**, 199–202.

Hodges, K.V. 2000. Tectonics of the Himalaya and southern Tibet from two perspectives. *Geological Society of America Bulletin*, **112**, 324–350.

Honegger, K., Dietrich, V., Frank, W., Gansser, A., Thöni, M. & Trommsdorf, V. 1982. Magmatism and metamorphism in the Ladakh Himalayas (the Indus–Tsangpo suture zone). *Earth and Planetary Science Letters*, **60**, 253–292.

Honegger, K., Le Fort, P., Mascle, G. & Zimmermann, J.-L. 1989. The blueschists along the Indus Suture Zone in Ladakh, NW Himalaya. *Journal of Metamorphic Geology*, **7**, 57–72.

Hubbard, M.S. & Harrison, T.M. 1989. $^{40}Ar/^{39}Ar$ age constraints on deformation and metamorphism in the Main Central Thrust zone and Tibetan Slab, eastern Nepal Himalaya. *Tectonics*, **8**, 865–880.

Hurford, A.J. 1990. Standardization of fission track dating calibration: recommendation by the Fission Track Working Group of the I.U.G.S. Subcommission on Geochronology. *Chemical Geology (Isotope Geoscience Section)*, **80**, 171–178.

Hurford, A.J. & Green, P.F. 1983. The Zeta age calibration of fission-track dating. *Chemical Geology (Isotope Geoscience Section)*, **41**, 285–317.

Laslett, G.M. & Galbraith, R. 1996. Statistical modelling of thermal annealing of fission tracks in apatite. *Geochimica et Cosmochimica Acta*, **60**, 5117–5131.

Linner, M., Fuchs, G., Koller, F. & Thöni, M. 2001. The Nidar Ophiolite within the Indus Suture Zone in eastern Ladakh—a marginal basin ophiolite from the Jurassic–Cretaceous boundary. *Journal of Asian Earth Sciences*, **19**, 39.

Maluski, H. & Matte, P. 1984. Ages of alpine tectonometamorphic events in the northwestern Himalaya (Northern Pakistan) by $^{40}Ar/^{39}Ar$ method. *Tectonics*, **3**, 1–18.

McDougall, I. & Harrison, M. 1988. *Geochronology by the $^{40}Ar/^{39}Ar$ Method*. Oxford Monographs on Geology and Geophysics, **9**.

Mukherjee, B.K. & Sachan, H.K. 2001. Discovery of coesite from Indian Himalaya: a record of ultra-high pressure metamorphism in Indian Continental Crust. *Current Science*, **81**, 1358–1361.

Schärer, U., Hamet, J. & Allègre, C.J. 1984. The transhimalaya (Gangdese) plutonism in the Ladakh region: a U–Pb and Rb–Sr study. *Earth and Planetary Science Letters*, **67**, 327–339.

Schlup, M. 2003. *Exhumation history of the western Himalaya: The Rupsha–Lahul–Kullu geochronological transect (NW India)*. PhD Thesis, University of Lausanne.

Sharma, K.K. 1991. Petrology, geochemistry and geochronology of the Ladakh batholith and its role in the evolution of Ladakh magmatic arc. *Physics and Chemistry of the Earth*, **17**, 173–194.

Sharma, K.K. & Choubey, V.M. 1983. Petrology, geochemistry and geochronology of the southern margin of the Ladakh batholith between Upshi and Chumatang. *In:* Thakur, V.C. & Sharma, K.K. (eds) *Geology of the Indus Suture Zone of Ladakh*. Wadia Institute of Himalayan Geology, Dehra Dun, India, 41–60.

Sinclair, H.D. & Jaffey, N. 2001. Sedimentology of the Indus Group, Ladakh, northern India: implications for the timing of initiation of the palaeo-Indus River. *Journal of the Geological Society, London*, **158**, 151–162.

Steck, A. & Spring, L. *et al.*1993. Geological transect across the northwestern Himalaya in eastern Ladakh and Lahul (a model for the continental collision of India and Asia). *Eclogae Geologicae Helvetiae*, **86**, 219–263.

Steck, A., Epard, J.-L., Vannay, J.-C., Hunziker, J., Girard, M., Morard, A. & Robyr, M. 1998. Geological transect across the Tso Morari and Spiti areas—the nappe structures of the Tethys Himalaya. *Eclogae Geologicae Helvetiae*, **91**, 103–121.

Stutz, E. & Thöni, M. 1987. The lower Palaeozoic Nyimaling granite in the

Indian Himalaya (Ladakh): new Rb–Sr data versus zircon typology. *Geologische Rundschau*, **76**, 307–315.

Tagami, T., Galbraith, R.F., Yamada, G.M. & Laslett, G.M. 1998. Revised annealing kinetics of fission-track in zircon and geological implications. *In:* Van den Haute, P. & De Corte, F. (eds) *Advances in Fission-track Geochronology*. Kluwer, Dordrecht, 99–112.

Thakur, V.C. & Misra, D.K. 1984. Tectonic framework of the Indus and Shyok suture zones in eastern Ladakh, Northwestern Himalaya. *Tectonophysics*, **101**, 207–220.

Thakur, V.C. & Virdi, N.S. 1979. Lithostratigraphy, structural framework, deformation and metamorphism of the southeastern region of Ladakh, Kashmir Himalaya, India. *Himalayan Geology*, **9**, 63–78.

Van Haver, T., Bonhomme, M.G., Mascle, G. & Aprahamian, J. 1986. Analyse K/Ar de phyllites fines des formations détritiques de l'Indus au Ladakh (Inde). Mise en évidence de l'âge Eocène supérieur du métamorphisme. *Comptes Rendues de l'Académie des Sciences*, **302**, 325–330.

Vannay, J.-C. & Grasemann, B. 1998. Inverted metamorphism in the High Himalaya of Himachal Pradesh (NW India): phase equilibria versus thermobarometry. *Schweizerische Mineralogische und Petrographische Mitteilungen*, **78**, 107–132.

Virdi, N.S., Thakur, V.C. & Kumar, S. 1977. Blueschist facies metamorphism from the Indus suture zone of Ladakh and its significance. *In:* Anshu, K. (ed.) *Himalayan Geology*. Wadia Institute of Himalayan Geology, Dehra Dun, India, 479–482.

Weinberg, R.F. & Dunlap, W.J. 2000. Growth and deformation of the Ladakh Batholith, Northwest Himalayas: implications for timing of continental collision and origin of calc-alkaline batholiths. *Journal of Geology*, **108**, 303–320.

White, N.M., Pringle, M., Garzanti, E., Bickle, M., Najman, Y., Chapman, H. & Friend, P. 2002. Constraints on the exhumation and erosion of the High Himalayan Slab, NW India, from foreland basin deposits. *Earth and Planetary Science Letters*, **195**, 22–44.

Wiesmayr, G. & Grasemann, B. 1999. Balanced cross-section and depth-to-detachment calculations for the Tethyan Himalaya (Spiti, N India): where is the crystalline basement of the Higher Himalaya? *Terra Nostra*, **9912**, 172–173.

Received 10 June 2002; revised typescript accepted 16 December 2002.
Scientific editing by Martin Whitehouse